Chapter 3. Gas Source Molecular Beam Epitaxy of Compound Semiconductors

Academic and Research Staff

Professor Leslie A. Kolodziejski, Dr. Gale S. Petrich

Graduate Students

Joseph F. Ahadian, Jay N. Damask, Easen Ho, Jody L. House, Kuo-Yi Lim, Elisabeth A. Marley, Jeremy M. Milikow, Steven G. Patterson, Xiao-feng Tang, Emily L. Warlick

Undergraduate Students

Anna Lopatnikova

Technical and Support Staff

Charmaine A. Cudjoe-Flanders, Angela R. Odoardi

3.1 Introduction

The emphasis of the research program which utilizes the chemical beam epitaxy laboratory revolves primarily around the epitaxial growth of a wide variety of compound semiconductors (both II-VI and III-V), as well as multilayered structures composed of II-VI/II-VI, II-VI/III-V and III-V/III-V heterostructures. The chemical beam epitaxy laboratory consists of two gaseous source epitaxy reactors (II-VI-dedicated and III-V-dedicated) interconnected to several smaller chambers which are used for sample introduction and *in-situ* surface analysis and metallization. Such a multichamber epitaxy system allows the fabrication of the aforementioned heterostructures to be accomplished within a continuous ultrahigh vacuum environment. The interconnected reactors enable an additional degree of freedom in device design by providing the ability to integrate the II-VI and III-V material families into a single device. For example, structures containing only III-V epilayers or only II-VI epilayers are grown in a single reactor, or in the case of II-VI/III-V heterostructures and quantum wells both reactors are used.

The III-V gas source molecular beam epitaxy (GSMBE) reactor uses solid elemental sources of Ga, In, Al, Si, and Be and gaseous hydride sources of arsenic and phosphorus. The II-VI reactor currently uses solid elemental sources of Zn and Se, as well as gaseous hydrogen selenide, in addition to a nitrogen plasma source and a solid $ZnCl_2$ source to achieve p- and n-type doping, respectively. The plasma source is also used with a high purity hydrogen/argon mixture for hydrogen plasma cleaning of GaAs and ZnSe substrates.

In the next section, we will describe our progress in the growth and doping of ZnSe using gas source molecular beam epitaxy and solid source molecular beam epitaxy to examine the role of hydrogen during epitaxy. The II-VI effort is complemented by a program investigating the growth of ZnSe on epitaxial (In,Ga,Al)P buffer layers. An additional II-VI/III-V effort involves the fabrication of ZnSe/GaAs quantum well structures, focusing on the formation of the ZnSe/III-V heterovalent structure and its resultant properties. The III-V GSMBE system is also utilized for the fabrication of (In,Ga)(As,P) waveguide-based devices and light emitters that operate at 1.55 μm, which is the wavelength used for optical fiber communication. Additional III-V-based projects include the fabrication of optoelectronic devices on premetallized GaAs MESFET integrated circuits for optoelectronic integrated circuits, and the fabrication of photonic bandgap crystals utilizing an air bridge microcavity structure. A final project consists of the fabrication of three-dimensional photonic bandgap crystals.

3.2 Gas Source Molecular Beam Epitaxy of ZnSe, ZnSe:Cl and ZnSe:N

Project Staff

Professor Leslie A. Kolodziejski, Dr. Gale S. Petrich, Easen Ho, Jody L. House, Emily L. Warlick, Anna Lopatnikova

Under the University Research Initiative (URI) program sponsored by ARPA through the Office of Naval Research, Professor Kolodziejski is a co-principal investigator along with Professor R.L. Gunshor, Purdue University, and Professor A.V. Nurmikko, Brown University. The focus of the URI is aimed towards achieving continuously operating, room temperature, short wavelength, visible light emitters operating in the blue and blue/green spectral ranges based on wide bandgap II-VI semiconductors. As the research effort continues toward eliminating the various technological barriers prohibiting the achievement of viable, commercial "blue" laser diodes, the heterostructures are becoming increasingly complex, requiring the use of advanced epitaxial growth techniques.

Gas source molecular beam epitaxy (GSMBE) is an alternative epitaxial growth method that replaces the high vapor pressure elements in molecular beam epitaxy (MBE) with hydride sources that are amenable to regulation using a precision mass flow controller. For example, AsH_3, PH_3, and H_2Se are used in place of elemental As, P, and Se, respectively, thus greatly reducing the associated problem of flux control. Lower vapor pressure elements such as Ga, In, and Zn are used in effusion sources. GSMBE retains most of the ultrahigh vacuum advantages of MBE while avoiding the use of metalorganic precursors and thus circumvents the issue of carbon incorporation. In addition, the use of a hydride gas cracker introduces an additional degree of freedom in controlling the form of the precursors provided to the growing surface. Several tradeoffs, however, are involved when using the GSMBE method, such as the high toxicity of the hydride gases and the increased pumping requirements compared to typical MBE apparatuses.

Another unique aspect of GSMBE is the copious and unavoidable generation of H_2 and sub-hydride species (such as As-H and Se-H) that are generated. Whether these H_2 and sub-hydride species are beneficial or deleterious depends on the material system involved. In the growth of III-V mate-

rials, the presence of hydrogen radicals have been postulated to aid in the removal of residual carbon inadvertently introduced into the vacuum system.[1] However, electrical passivation of both intentional and unintentionally introduced dopants has been frequently observed in the growth of Si and III-V compound materials. Our previous results[2] have shown that while the activation of chlorine donors in n-type ZnSe is not affected by the use of the H_2Se precursor, nitrogen-doped ZnSe is strongly passivated by hydrogen and leads to epitaxial layers that are electrically insulating. Secondary ion mass spectrometry (SIMS) analysis of both the chlorine-doped and nitrogen-doped ZnSe further confirmed the preferential electrical passivation of nitrogen by hydrogen. While the hydrogen concentration, [H], and chlorine concentration, [Cl], were found to behave independently of each other in the chlorine-doped samples, the clear synergy between the hydrogen concentration [H] and the nitrogen concentration [N] were observed in SIMS depth profiling (see figure 1).

An important question that remains to be answered concerns the passivation that is observed during the GSMBE growth of ZnSe doped with a nitrogen plasma source, i.e., is the *dominant* source of electrical passivation derived from molecular hydrogen that is produced by cracking, or from hydrogen radicals still attached to the Se precursor? In order to quantify the role of molecular hydrogen in the passivation mechanism of nitrogen acceptors, experiments were undertaken where various amounts of hydrogen were introduced into the chamber during conventional MBE growth. Figure 2 shows a SIMS profile of a structure containing intentionally hydrogenated regions (lined regions in the structure schematic) where different amounts of molecular hydrogen were introduced; the layer also contains undoped regions (shaded regions) as well as a doped region that was not exposed to a flux of hydrogen. The main features to note in figure 2 are as follows: (1) similar to GSMBE-grown ZnSe:N, [H] is seen to closely track [N], with both impurities decreasing to near their background levels in all of the undoped regions; (2) a clear increase in [H] coincident with the addition of 1 SCCM H_2 (from the schematically indicated ZnSe:N region to the ZnSe:N + 1.0 SCCM H_2 region) indicates that *nitrogen-induced hydrogen incorporation* has occurred; and (3) the [N]/[H] ratio in the ZnSe:N +

1 Y. Okada, T. Sugaya, O. Shigeru, T. Fujita, and M. Kawabe, "Atomic Hydrogen-assisted GaAs Molecular Beam Epitaxy," *Jpn. J. Appl. Phys.* 34(2B): L238-L244 (1995); M. Sato, "Effect of Plasma-generated Hydrogen Radicals on the Growth of GaAs using Trimethylgallium," *Jpn. J. Appl. Phys.* 34(1B): L93-L96 (1995).

2 E. Ho, P.A. Fisher, J.L. House, G.S. Petrich, L.A. Kolodziejski, J. Walker, and N.M. Johnson, "Hydrogen Passivation in Nitrogen and Chlorine-doped ZnSe Films Grown by Gas Source Molecular Beam Epitaxy," *Appl. Phys. Lett.* 66(9): 1062-1064 (1995).
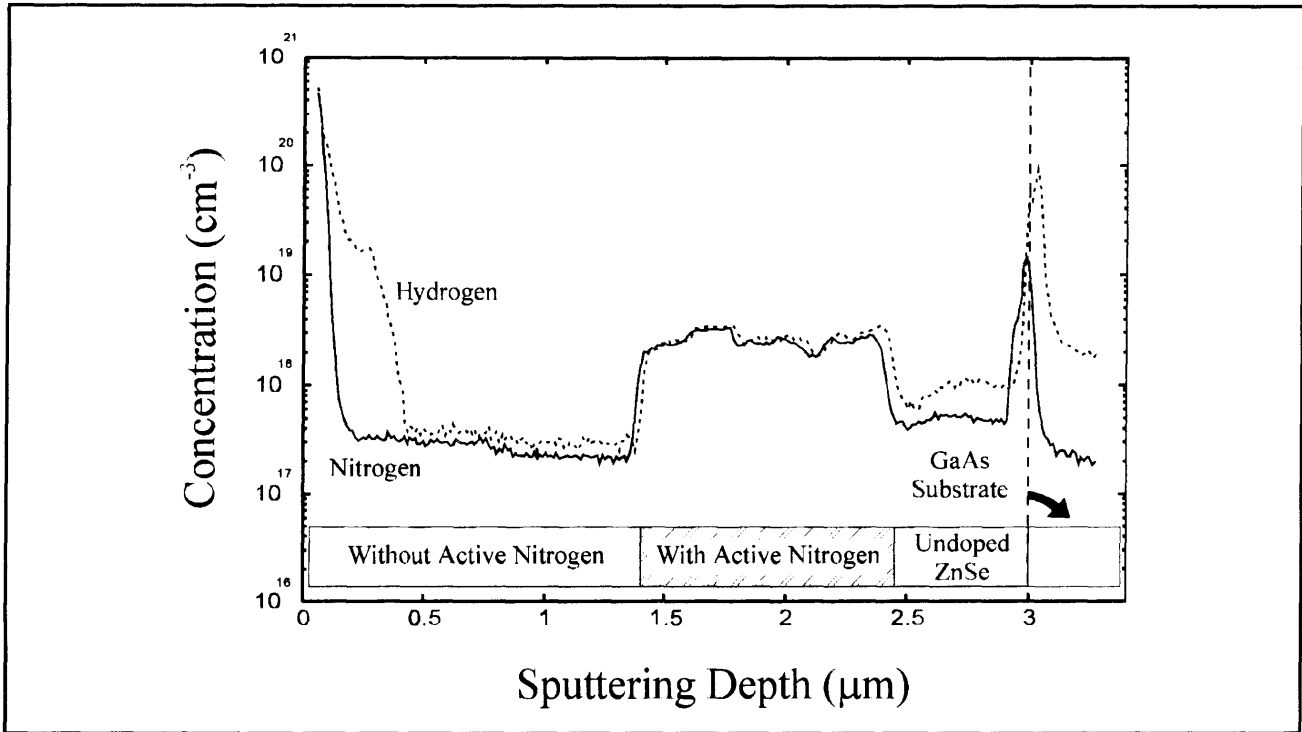
Figure 1. SIMS profile of a layered structure with designed nitrogen concentration variations to demonstrate the tracking behavior of [H] with [N]. The abrupt increases in the [H] and [N] near the ZnSe/GaAs interface were artifacts of the data normalization procedure and should be ignored.

1.0 SCCM region appears to be greater than the [N]/[H] in the ZnSe:N + 3.5 SCCM H_2 region which is consistent with the assumption that the observed increase in [H] is directly related to the amount of injected H_2.[3]

A comparison of capacitance-voltage (C-V) measurements performed on unhydrogenated ZnSe:N films (reference films without H_2) and intentionally hydrogenated films (ZnSe:N + various amounts of H_2) lends further support to our hypothesis that molecular hydrogen acts to passivate the nitrogen acceptors in MBE using a nitrogen plasma cell. Several series of nitrogen-doped films were grown by MBE, both with and without intentional hydrogen, using identical growth and doping conditions. C-V measurements were subsequently performed on all of the samples to measure the net acceptor concentration [$N_A - N_D$]. With a target [$N_A - N_D$] of $\sim 2 \times 10^{17}\,cm^{-3}$ for the unhydrogenated reference samples (typical MBE growth), it was generally found that a significant decrease in [$N_A - N_D$] occurred for films that were grown with injected hydrogen. As an example of the magnitudes of

passivation that were observed, 25 percent and 60 percent passivation were measured for flow rates of 1 and 2 SCCM of H_2, respectively, as compared to the reference (unhydrogenated) MBE-grown samples (where the passivation was taken to be the 0 percent reference). This particular set of hydrogenation runs were grown at 280°C, under slightly Se-rich conditions with the following RF source parameters: 400 W of power and 2.2×10^{-5} Torr chamber background N_2 pressure. The precise amount of passivation was found to depend on the growth, doping conditions, as well as the hydrogen flow rates that were used. Figure 3 shows a *normalized percent passivation* (normalized by the nitrogen doping parameter defined as the product of *power * pressure*) as a function of the hydrogen flow rate used during the hydrogenation experiments. The positive slope in figure 3 highlights a result that we would reasonably expect: more hydrogen present at the surface *for a given amount of active nitrogen* species gives rise to a larger degree of observed passivation. Note that it is the relative amount of passivation that is of interest here and not the absolute magnitudes. The

---

3 The apparent increase in [H] at the interface of undoped ZnSe and ZnSe:N regions is due to residual levels of hydrogen in the shared hydrogen/nitrogen gas manifold that feeds the RF plasma cell. Therefore, some background level of passivation exists for this particular experiment even though H_2 is not intentionally introduced via the cracker.
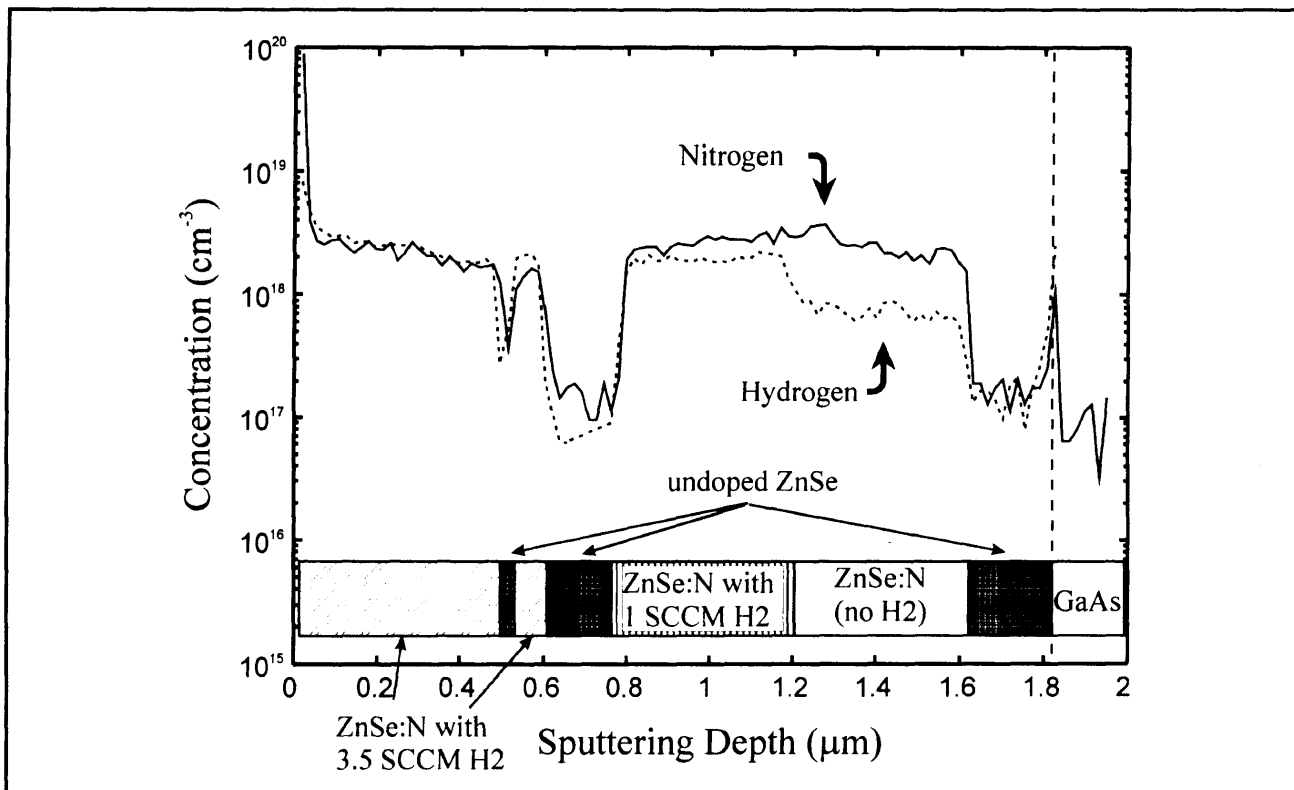
Figure 2. SIMS profile of a ZnSe:N layer grown by MBE on an undoped ZnSe buffer layer (on GaAs). As the depth into the ZnSe layer increases, various amounts of H_2 were introduced to the growth front, with two undoped regions as indicated. The undoped regions serve as markers for the background [H] and [N] concentrations. Variations in the H_2 flow are as indicated in the figure.

result of figure 3 can also be stated in a corollary manner: the amount of electrical passivation depends on the amount of active nitrogen present *for a given flow of hydrogen.* These results and postulates advanced above are consistent with the recent data on the thermal annealing of MOVPE-grown ZnSe:N films obtained by Ogata et al.,[4] where annealing ZnSe:N epilayers (possessing an initial net acceptor concentration of 2.0×10^{17} cm^{-3}) in an H_2 ambient at 350°C was found to provide significant electrical passivation of the nitrogen acceptors. More detailed studies are required to quantitatively understand the passivating relationship between the active nitrogen species and the H_2 present at the growing surface.

Cracking experiments with H_2Se revealed that 2 SCCM of injected H_2 provides a background hydrogen signal (as detected using a quadrupole mass spectrometer) that is approximately equal to that normally encountered during normal GSMBE growth. Since the degree of electrical passivation
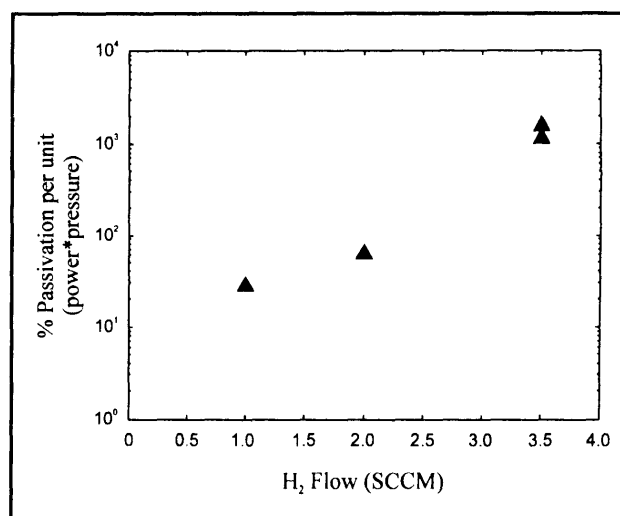
Figure 3. The percent of acceptor passivation (normalized by the doping parameter defined as the product of *power * pressure*) as a function of the intentionally injected H_2 flow rate.

4 K. Ogata, D. Kawaguchi, T. Kera, Sz. Fujita, and Sg. Fujita, paper presented at the Seventh International Conference on II-VI Compounds and Devices, Edinburgh, Scotland, August 13-18, 1995.

of GSMBE-grown ZnSe:N samples is found to be much more significant than that measured for the MBE + H_2 counterparts exposed to similar H_2 background levels, we speculate that an equally important mechanism for nitrogen acceptor passivation is related to incompletely cracked Se-H fragments. It is expected that hydrogen passivation during GSMBE growth can be *minimized* by cracking the H_2Se precursor as completely as possible. However, our results seem to indicate that some passivation is inevitable due to the presence of H_2 under normal growth and stoichiometry conditions. This reasoning might also play a part in reconciling our present results with other seemingly contradictory results,[5] where hydrogen passivation has been reported to be absent in GSMBE-grown ZnSe using the same precursors. We believe that the hydrogenation behavior described here has significant implications for the GSMBE, as well as MOVPE growth of ZnSe:N where multiple pathways for hydrogen incorporation may exist. Further experiments are currently underway to study the effect of growth and surface stoichiometry conditions on hydrogen incorporation under both MBE and GSMBE growth conditions. It is our belief that further and fundamental understanding of the surface kinetic reactions that occur with hydrogen during GSMBE and MOVPE will ultimately dictate the usefulness of GSMBE and MOVPE for achieving practical and reproducible p-type conductivity in wide bandgap II-VIs with nitrogen acceptors.

3.2.1 Publications

Fisher, P.A., E. Ho, J.L. House, G.S. Petrich, L.A. Kolodziejski, J. Walker, and N.M. Johnson. "P- and N-type Doping of ZnSe: Effects of Hydrogen Incorporation." Eighth International Conference on Molecular Beam Epitaxy, Osaka, Japan, August 29-September 2, 1994; In *J. Cryst. Growth* 105(1-4): 729-733 (1995).

Ho, E., P.A. Fisher, J.L. House, G.S. Petrich, L.A. Kolodziejski, J. Walker, and N.M. Johnson. "Hydrogen Passivation in Nitrogen- and Chlorine-Doped ZnSe Films Grown by Gas Source Molecular Beam Epitaxy." *Appl. Phys. Lett.* 66(9): 1062-1064 (1995).

Ho, E., G.S. Petrich, and L.A. Kolodziejski. "Comparison of Hydrogen Passivation of ZnSe:N

Using Gas Source and Conventional Molecular Beam Epitaxy." Paper presented at the Seventh International Conference on II-VI Compounds and Devices, Edinburgh, Scotland, August 13-18, 1995; *J. Cryst. Growth.* Forthcoming.

3.3 Novel Epitaxial III-V Buffer Layers for Wide Bandgap II-VI Visible Sources

Sponsors

Project Staff

Professor Leslie A. Kolodziejski, Dr. Gale S. Petrich, Easen Ho, Jody L. House, Emily L. Warlick

At present, most research into II-VI light emitting devices involves the use of GaAs substrates. GaAs is less expensive and more readily available than bulk ZnSe substrates, and allows for the eventual integration of II-VI optical devices onto GaAs-based electronics. Light-emitting diodes are described by the basic concepts of a forward biased pn-junction diode. By forward biasing the pn-junction, holes that are injected from the p-type region into the n-type region, recombine with electrons, resulting in photon emission. However, several mechanisms reduce the amount of radiative recombination due to the use of GaAs substrates, including non-radiative recombination due to misfit dislocations that are generated because of the 0.27 percent lattice-mismatch between ZnSe and GaAs, and the difficulty of injecting holes into the II-VI layers due to the large valence band discontinuity between the two semiconductors.

The lattice-mismatch between the ZnSe epilayer and the GaAs substrate causes a high density of misfit dislocations to form when the ZnSe epilayer thickness exceeds the critical layer thickness (150 nm for ZnSe on GaAs). The presence of misfit dislocations and stacking faults that occur at the II-VI/III-V interface causes the formation of new defects which propagate within the device and act

5 M. Imaizumi, Y. Endoh, K. Ohstuka, T. Isu, and M. Nunoshita, "Active-nitrogen Doped P-type ZnSe Grown by Gas Source Molecular Beam Epitaxy," *Jpn. J. Appl. Phys.* 32(12A): L1725-L1727 (1994); M. Imaizumi, Y. Endoh, K. Ohstuka, M. Suita, T. Isu, and M. Nunoshita, "Blue Light Emitting Laser Diodes Based on ZnSe/ZnCdSe Structures Grown by Gas Source Molecular Beam Epitaxy," *Jpn. J. Appl. Phys.* 33(1A): L13-L14 (1994).

as nonradiative recombination centers.[6] The forma-
tion of the new nonradiative recombination centers
leads to the degradation of the device. By varying
the mole fraction of In, (In,Ga)P can be designed to
be lattice-matched to ZnSe as opposed to GaAs,
thus minimizing the strain-induced misfit dislo-
cations between the ZnSe and the (In,Ga)P.[7]

The second problem with a GaAs substrate is the
valence band offset between the ZnSe and the
GaAs. The valence band discontinuities between
ZnSe and GaAs, InGaP, and InAlP are 0.96 eV,
0.67 eV, and 0.34 eV, respectively. The reduction
of the heterobarrier with an intermediate (In,Ga)P
buffer layer has been found to lead to an enhance-
ment of the hole thermionic emission,[8] which in turn
improved the electrical characteristics of the device.

At present, structures of the form
ZnSe/(In,Ga,Al)P/GaAs are being studied, as shown
in figure 4. The specific buffer layers studied
include InGaP, InAlP, and graded layers of
In(Ga,Al)P. As shown schematically in the upper
part of figure 4, by varying the Ga to Al ratio in
In(Ga,Al)P, the valence band offset between the
ZnSe and the III-V epilayer can be decreased as
the (In,Ga,Al)P bandgap energy increases. This
can be accomplished independent of the lattice

constant. The lattice constant of the epilayers were
either equal to the lattice constant of ZnSe or
graded from the GaAs lattice constant to the lattice
constant of ZnSe during the growth of the epilayer
as shown in the bottom of figure 4. In doing so, the
lattice mismatch between the III-V epilayer and the
ZnSe layer can be minimized. The III-V buffer
layers were transferred in-situ to the II-VI chamber.
In the III-V GSMBE reactor, the In(Ga,Al)P buffer
layers were grown with cracked arsine (AsH₃) and
phosphine (PH₃) as the anion species, and ele-
mental In, Ga, and Al as the cation species. The 4
μm thick buffer layers were grown at 490°C on an
epitaxial 0.5 μm thick GaAs buffer layer, which was
grown at 600°C. The 1 μm thick ZnSe layers were
grown using elemental Zn and Se as source mate-
rials at a temperature around 300°C.

Several characterization techniques have been
employed to investigate these epitaxial
In(Ga,Al)P/ZnSe heterostructures, including in-situ
reflection high energy electron diffraction (RHEED),
Nomarski microscopy, x-ray diffraction (XRD), pho-
toluminescence (PL), and cathodoluminescence
(CL). XRD yielded information about the lattice
matching as well as the dislocation density from the
width of the diffraction peaks.[9] The (400) diffraction
rocking curves indicated that all of the (In,Ga,Al)P
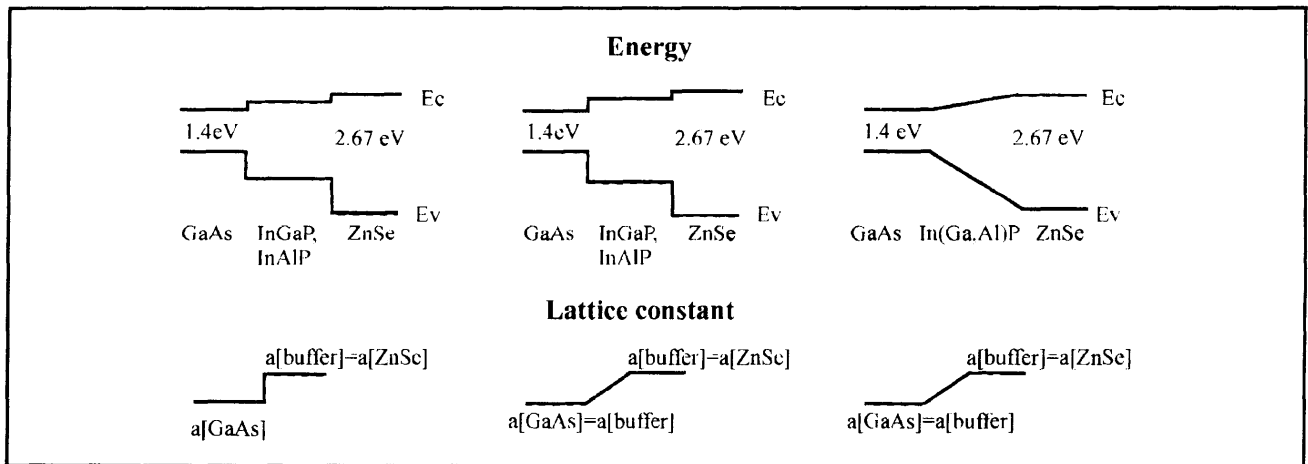
Figure 4. Schematic diagrams of the energy bands and lattice-constants of the In(Ga,Al)P/ZnSe heterostructures.

6 S. Guha, J.M. DePuydt, M.A. Haase, J. Qiu, and H. Cheng, "Degradation of II-VI Based Blue-green Light Emitters," Appl. Phys. Lett.
63(23): 3107-3109 (1993); S. Guha, H. Cheng, M.A. Haase, J.M. DePuydt, J. Qiu, B.J. Wu, and G.E. Hofler, "<100> Dark Line
Defect in II-VI Blue-green Light Emitters," Appl. Phys. Lett. 65(7): 801-803 (1994).

7 K. Lu, J.L. House, P.A. Fisher, C.A. Coronado, E. Ho, G.S. Petrich, and L.A. Kolodziejski, "(In,Ga)P Buffer Layers for ZnSe-Based
Visible Emitters," J. Cryst. Growth 138(1-4): 1-7 (1994).

8 M. Onomura, M. Ishikawa, Y. Nishikawa, S. Saito, P.J. Parbrook, K. Nitta, J. Rennie, and G. Hatakoshi, "Blue-green Laser Diode
Operation of CdZnSe/ZnSe MQW Structures Grown on InGaP Band Offset Reduction Layers," Electron. Lett. 29(24): 2114-2115
(1993).

9 R.L. Gunshor, N. Otsuka, and A.V. Nurmikko, "Blue Lasers on the Horizon," IEEE Spectrum 30(5): 28-33 (1993).

buffer layers were lattice-matched to ZnSe to within an average of 100 arcseconds. CL provides a spatial image of the luminescence of the semiconductor. In imaging of defects, the CL contrast is generally due to the enhanced nonradiative recombination at dislocations in the crystal. In undoped semiconductors used in this study, threading dislocations appear as very dark dots.[10] These can clearly be seen in figure 5.

Currently, work is underway to image the defects in the structures using transmission electron microscopy (TEM) in order to determine the relative prominence of various forms of dislocations and faults. These results will enhance our understanding of the specific effects of lattice-matching. Eventually, the structures will be doped p-type with an n-type layer of ZnSe on top to perform I-V measurements and to evaluate the electrical capabilities of the diodes.

## 3.4 The Growth and Characterization of ZnSe/GaAs Heterostructures

Project Staff

Professor Erich P. Ippen, Professor Leslie A. Kolodziejski, Dr. Gale S. Petrich, David J. Dougherty, Jody L. House

The integration of II-VI and III-V semiconductors into a single II-VI/III-V heterojunction device enables the exploitation of the many similarities, as well as the many differences, in material properties (energy bandgap, lattice constant, dielectric constant, etc.) to create new devices exhibiting unique optical and electronic properties. As a specific example, the epitaxial growth of dielectric quantum wells (QWs) composed of ZnSe (E_g=2.67eV) and GaAs (E_g=1.42 eV) is under investigation. ZnSe and GaAs have very similar lattice constants (0.27 percent lattice
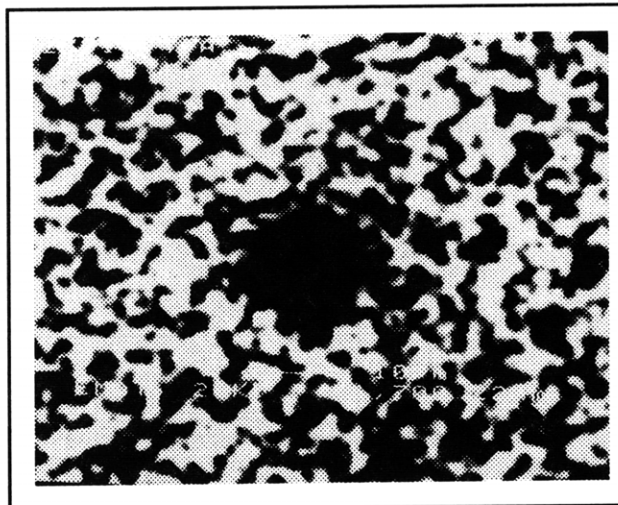
Figure 5. Room-temperature cathodoluminescence image of ZnSe/InAlP/GaAs, where the InAlP was lattice-matched to ZnSe. The image was taken at the peak wavelength of 460 nm. The bright regions are luminescent; the dark spots show points of nonradiative recombination, due primarily to threading dislocations.

mismatch) which enable the materials to be grown epitaxially to form a heterostructure.

A quantum well consisting of a thin layer of GaAs (1 - 100 nm) surrounded by ZnSe barriers has a large potential well (~1 eV) in the valence band for holes and a smaller potential well (~0.2 eV) in the conduction band for the electrons. Such a large potential barrier for the holes results in a number of possible confined hole energy states in the GaAs quantum well. When such a ZnSe/GaAs quantum well is excited, either electrically or optically, the transitions of holes between these confined levels (intersubband transitions) in the valence band can be detected. Furthermore, from a ZnSe/GaAs multiple quantum well structure, the density of intersubband transitions for the holes can be engineered to achieve a large signal at the optical communications wavelength of 1.3 μm. In addition, the large variation in the other optical properties of GaAs and ZnSe (including a variation in the index of refraction of ~1) makes the mixed II-VI/III-V heterostructure a candidate for high-speed optical switching devices (switching times of less than 1 picosecond).[11]

---

10 B.G. Yacobi and D.B. Holt, "Cathodoluminescence Scanning Electron Microscopy of Semiconductors," *J. Appl. Phys.* 59(4): R1-R24 (1986).

11 H. Buhmann, L. Mansouri, J. Wang, P.H. Beton, L. Eaves, and M. Henini, "High Efficiency Submicron Light-emitting Resonant Tunneling Diodes," *Appl. Phys. Lett.* 65(26): 3332-3334 (1994); O.E. Raichev, "Theory of Hole Conductivity in Semiconductor Superlattices," *Phys. Rev. B* 50(8): 5382-5391 (1994); M. Kumagai and T. Takagahara, "Excitonic and Nonlinear-optical Properties of Dielectric Quantum-well Structures," *Phys. Rev. B* 40(18): 12,359-12,381 (1989); J. Moores, K. Bergman, H.A. Haus, and E.P. Ippen, "Optical Switching Using Fiber Ring Reflectors," *J. Opt. Soc. B* 8(3): 594-601 (1991); K. Kitayama and S. Wang, "Optical Pulse

A heterostructure intended for device purposes needs to have well-defined characteristics. In the ZnSe and GaAs case, there are two issues which affect the properties of the heterointerfacial regions. First, the GaAs and ZnSe are composed of elements with different valences. As one material is formed on top of the other, the bonding of the four different elements can have several orientations. For example, a theoretically abrupt interface can be formed where there are no interfacial layers of Ga, Zn, Se, and As. In this instance, an electronic imbalance results, and the associated electric field creates a depletion region for stability. In the instance when a few transitional monolayers exist, the heterostructure is no longer entirely ZnSe and GaAs. One goal of this study is to determine which of these two extremes is the best from a device perspective. There has been a great deal of work to date in defining the electronic structure of the ZnSe on GaAs heterostructure. Theoretically, the valence band-offset between the ZnSe and the GaAs has been shown to vary from 0.7 eV to 1.59 eV, depending on the ZnSe/GaAs interface formation.[12] However, little is known about the far-reaching effects of these different interfaces.

The second issue affecting the properties of the ZnSe/GaAs QW structure is the formation of the heterovalent interfaces, particularly the formation of the inverted interface formed by GaAs nucleated on a ZnSe epitaxial surface. The stoichiometry of each interface is engineered by using various growth techniques. Due to the severe mismatch in the optimal growth temperatures for the two material systems (600°C for GaAs and 300°C for ZnSe), additional emphasis has been placed on the reduced temperature growth of GaAs on ZnSe.

The nucleation of GaAs on ZnSe has been optimized utilizing a monolayer by monolayer growth procedure. The substrate temperature was increased from 250°C to 350°C while the V-III flux ratio was decreased from 12 to approximately one

during the deposition of the first ten monolayers. This approach has resulted in a defect-free heterointerface as exhibited in cross-sectional TEM micrographs (figure 6a). *In situ* monitoring of the GaAs nucleation on ZnSe with reflection high energy electron diffraction has shown a reconstructed c(4x4) surface within six monolayers of GaAs, indicating a smooth As-rich GaAs surface. For comparison, MBE-like nucleation conditions that were employed for the nucleation of GaAs on ZnSe (where the substrate temperature was 370°C and the V-III flux ratio was approximately five) resulted in a heterointerface riddled with a high density of stacking faults which propagate through the GaAs material as shown in figure 6b. The RHEED pattern for the MBE-like nucleation of GaAs on ZnSe exhibited a spotty bulk-like diffraction pattern indicative of a rough surface.

Optical characterization has been implemented to assess the quality of the reduced temperature GaAs and the ZnSe/GaAs double heterostructures. Multiple quantum well heterostructures composed of (In,Ga)P barriers and GaAs wells exhibit low temperature photoluminescence from the first confined state of GaAs grown at temperatures as low as 300°C. The optical properties of the ZnSe/GaAs double heterostructure on both GaAs and InGaP buffer layers are under investigation with photoluminescence, photoreflectance, and photocurrent measurements. In addition, to examine the role of II-VI/III-V heterointerface, asymmetric quantum wells utilizing ZnSe and InGaP as barrier material, are also being investigated.

3.4.1 Publications

House, J.L., D.J. Dougherty, G.S. Petrich, L.A. Kolodziejski, E.P. Ippen, and G.-C. Hua. "Growth and Characterization of ZnSe/GaAs Single Quantum Well Structures." *Appl. Surf. Sci.* Forthcoming.

Compression by Nonlinear Coupling," *Appl. Phys. Lett.* 43(1): 17-19 (1983); N.M. Islam, *Ultrafast Fiber Switching Devices and Systems* (Cambridge, England: Cambridge University Press, 1992).

[12] G. Bratina, R. Nicolini, L. Sorba, L. Vanzetti, G. Mula, X. Yu, and A. Franciosi, "ZnSe-GaAs Heterojunction Parameters," *J. Cryst. Growth* 127(1-4): 387-391 (1993); G. Bratina, L. Vanzetti, R. Nicolini, L. Sorba, X. Yu, A. Franciosi, G. Mula, and A. Mura, "Microscopic Control of ZnSe-GaAs Heterojunction Band Offsets," *Physica B* 185(1-4): 557-565 (1993); G. Bratina, L. Vanzetti, L. Sorba, G. Biasiol, A. Franciosi, M. Peressi, and S. Baroni, "Lack of Band-offset Transitivity for Semiconductor Heterojunctions with Polar Orientation: ZnSe-Ge(001), Ge-GaAs(001), and ZnSe-GaAs(001)," *Phys. Rev. B* 50(16): 723-729 (1994); A. Kley and J. Neugebauer, "Atomic and Electronic Structure of the GaAs/ZnSe(001) Interface," *Phys. Rev. B* 50(12): 8616-8628 (1994); R. Nicolini, L. Vanzetti, G. Mula, G. Bratina, L. Sorba, A. Mura, J.E. Angelo, W.W. Gerberich, and A. Franciosi, "Local Interface Composition and Band Offset Tuning in ZnSe-GaAs(001) Heterostructures," *Phys. Rev. Lett.* 72(2): 294-297 (1994).

ZnSe

GaAs

ZnSe

200 Å
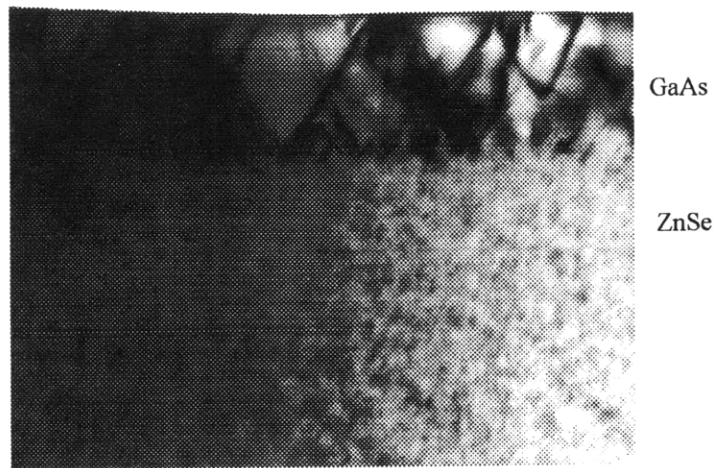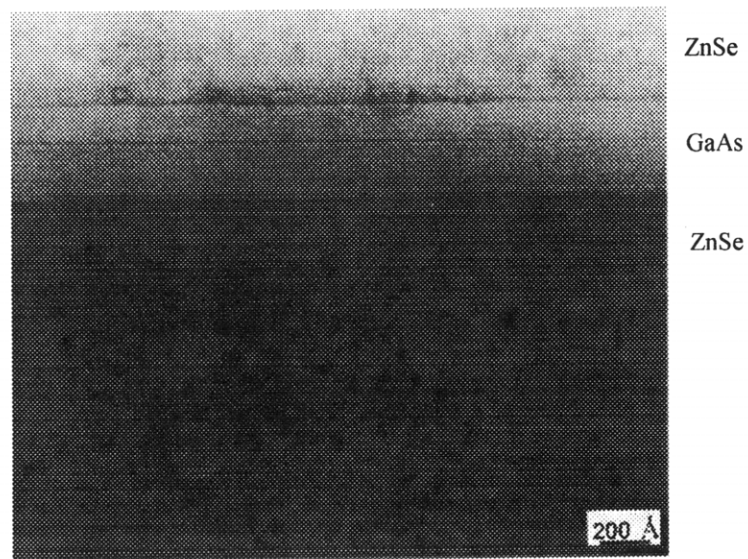
GaAs

ZnSe

Figure 6. Cross-sectional transmission electron micrographs of GaAs nucleated on an epitaxial ZnSe surface. (a) (top) A ZnSe/GaAs quantum well structure (500 Å ZnSe/ 400 Å GaAs /ZnSe substrate) that was formed using monolayer-controlled deposition. (b) (bottom) A 2500 Å GaAs layer that was nucleated on a ZnSe epilayer using typical MBE growth techniques.

3.5 Low Temperature Growth of (In,Ga)P/(In,Ga)As Lasers and LEDs for OptoElectronic-VLSI

Sponsor

National Center for Integrated Photonic Technology
Contract 542-381

Project Staff

Professor Clifton G. Fonstad, Jr., Professor Leslie A. Kolodziejski, Dr. Gale S. Petrich, Joseph F. Ahadian, Steven G. Patterson, Dr. Krishna V. Shenoy

We are investigating the regrowth of (In,Ga)As quantum well lasers and light emitting diodes (LEDs) onto premetallized GaAs-based VLSI circuits. Our approach involves the use of (In,Ga)P cladding layers with (In,Ga)As active regions (all lattice-matched to GaAs). Following the design of the VLSI MESFET circuits, Vitesse Corporation completes the fabrication including all levels of metalization of the electronic portion of the circuit using the MOSIS foundry. The last process step carried out by Vitesse involves the removal of the various layers of dielectric material from the growth window in order to create a region for the epitaxial regrowth of the optical components (lasers and LEDs); the samples are then forwarded to MIT for regrowth and optical device processing.

We are emphasizing the gas source molecular beam epitaxial growth of lasers, LEDs, and dielectric Bragg reflecting mirrors with the requirement that all of the growth and subsequent device processing is carried out at temperatures below 500°C. Temperatures greater than 500°C have been found to significantly degrade the upper level metal on the various electronic components within the VLSI circuitry. Initial GSMBE experiments involved the growth on both bulk GaAs substrates as well as in the growth window of the GaAs-based VLSI circuits. However, early results indicated that the processing steps that were used to remove the dielectric material from the growth window resulted in an unacceptable surface for the regrowth of high quality GaAs. The "regrown" material was found to be heavily defective and exhibited a very rough surface morphology. Subsequent device design and further processing experiments were required to modify the steps necessary to prepare the growth windows for epitaxy. A significant effort within Professor Fonstad's group has been expended to alleviate this surface preparation problem. While this surface preparation problem was being addressed, we initiated a parallel effort to determine the growth parameters necessary to fabricate the various optical components of interest onto bulk GaAs sub-

strate material. The results from these initial growth, characterization, and prototype device fabrication experiments will provide the optical device operating characteristics to our collaborators as part of the OPTOCHIP project. With the current-voltage, light output-current, threshold current and threshold voltage characteristics, further OE-VLSI designs will be implemented by our OPTOCHIP collaborators. In addition, these initial device results will provide a baseline for the optical components that are integrated with the OE-VLSI circuits. Material has also been forwarded to Lincoln Laboratory and to Professor Steve Forrest (Princeton University) to begin experiments to identify the processing chemistry necessary to form chemically-etched 45° folded cavity mirrors with reactive ion etching (Princeton) and parabolic mirrors using chemically-assisted ion beam etching (Lincoln Laboratory) for the final fabrication of in-plane surface emitting lasers fully integrated with the OE-VLSI circuits.

Using the integrated modular GSMBE reactors, we have eliminated the need to remove the native GaAs oxide by raising the substrate temperature to 650°C for several minutes prior to the initiation of growth. This is accomplished within the II-VI reactor by using atomic hydrogen from a plasma source for the low temperature removal of the GaAs oxide. The oxide is removed at 300°C in conjunction with a 15-30 minute exposure to atomic hydrogen. Since this initial success with the plasma source in the II-VI reactor, a source of atomic hydrogen has been added to the III-V reactor to enable the oxide removal to be carried out with an arsenic ambient to further reduce the difficulty of Ga-droplet formation due to the excess evaporation of arsenic.

For use in vertical cavity surface emitting laser structures (VCSELs) and high efficiency LEDs, we have grown various Bragg mirrors having both large and small index of refraction discontinuities. The structures consist of AlAs/(In,Ga)P, which exhibits a small index of refraction difference (figure 7), and Al_xO_y/(In,Ga)P which exhibits a large index difference. The lattice-matched Bragg mirrors exhibit high optical reflectivity at the wavelength of interest for the optical devices under consideration, but exhibit poor electrical characteristics. The low temperature (470°C) growth of the AlAs layer is speculated to contribute to the high electrical resistivity of the Bragg mirrors, thus negating the expected improvement in the efficiency of the LEDs. For the Al_xO_y/(In,Ga)P Bragg mirrors, we have established the oxidation conditions necessary to complete the oxidation of the AlAs/(In,Ga)P Bragg mirrors following the approach of Professor Dan Dapkus (University of Southern California). A fully functioning oxidation furnace has been assembled at MIT and
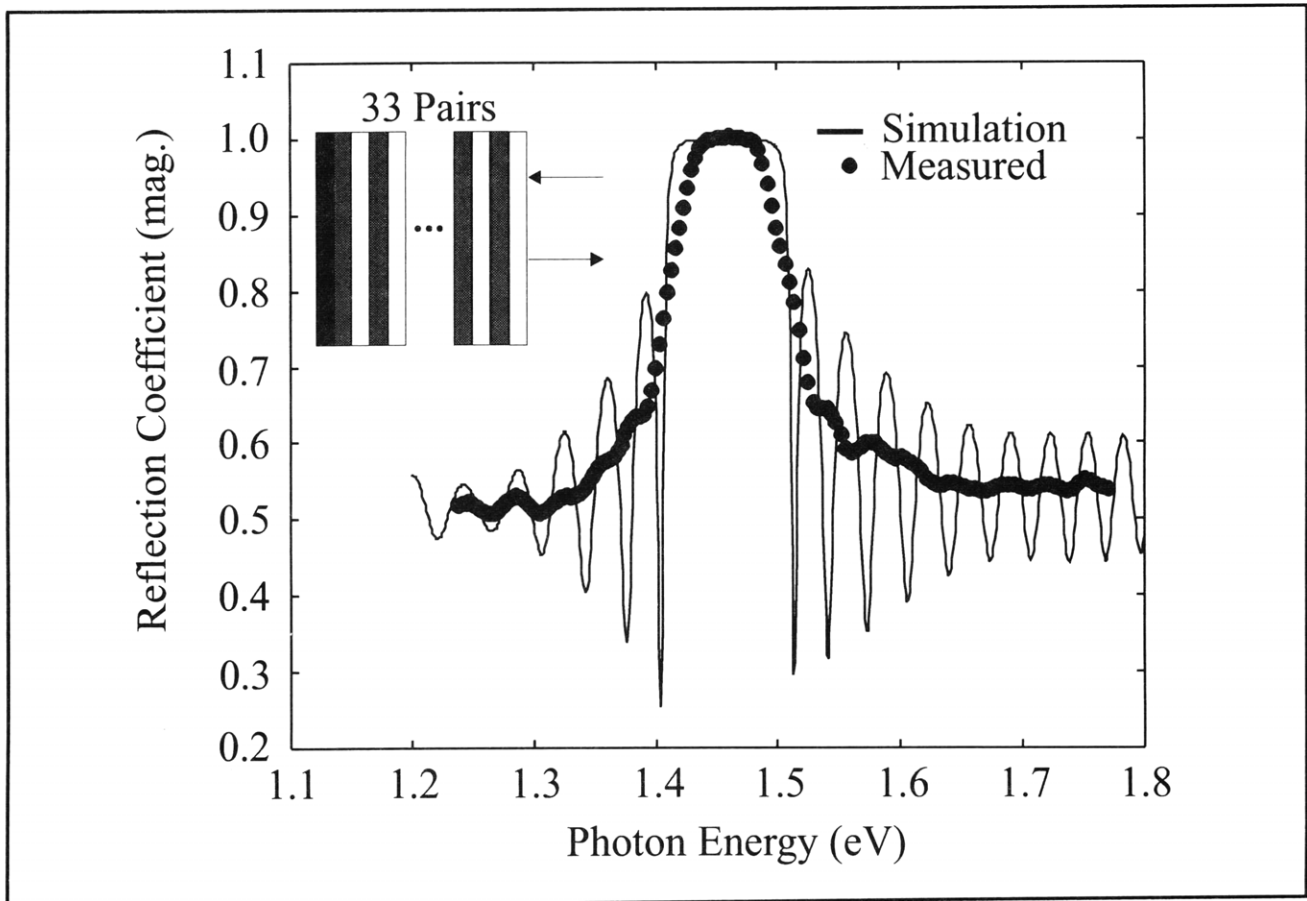
Figure 7. Measured and simulated reflection coefficient of a 33 pair InGaP/AlAs distributed Bragg reflector grown at 470°C on a GaAs substrate.

has been calibrated for the proper oxidation conditions. However, the oxidation temperature still needs to be reduced as the most successful oxidation conditions occur at 500°C, which exceeds the maximum allowable temperature during the processing of the optical devices with the integrated circuits.

A significant number of LEDs have been grown, fabricated, and characterized, each having various modifications to the layer design, doping characteristics, presence of etch stop layers, etc., to optimize the light emission from the optical device. The use of an AlAs etch stop layer was implemented to facilitate the chemical etching of the various sized mesas in order to minimize the leakage currents under a small forward bias.

To maximize the amount of light emitted from the LED structures, we are investigating various methods to increase the degree of current spreading underneath a top metal contact. Doping profile simulations of LED structures are being utilized to guide the growth experiments. In addition, we are investigating the use of alternative metal contacts, including transparent metal contacts, such

as Ti:Au in conjunction with current confining apertures, and transparent indium tin oxide contacts.

Thus far, various mask sets have been designed in order to vary the ratio of metal contact to surface area to maximize the light emission, but device fabrication is still required for proof of concept. In addition, the progress in fabricating LEDs using InGaP cladding layers, has been hampered by the wet chemical etching of the InGaP surfaces using $H_3PO_4/HCl/H_2O$. This etchant creates an etched surface with a rough morphology. We are currently investigating the use of $CH_3COOH/HCl/H_2O_2$. This etchant produces a smooth etched surface but causes process complications due to the presence of the organic acid.

Promising results have been demonstrated with regard to the cleaning steps necessary to prepare the growth windows for epitaxial regrowth. The new process involves a simple etch step by Vitesse to remove the various layers of dielectric down to a layer of Al that is placed near the final GaAs surface. Once the sample arrives at MIT, the aluminum layer is removed and the sample is then dipped in HF. The surface appears to be free of

the residue plaguing the earlier circuits, but still requires additional surface examination to determine the efficacy of this new surface cleaning process.

3.6 InP-Based Devices for Optical Communication Networks

Sponsors

MIT Lincoln Laboratory
National Center for Integrated Photonic Technology
    Subcontract 542-383

Project Staff

Professor Leslie A. Kolodziejski, Dr. Gale S. Petrich, Dr. Katherine L. Hall,[13] Dr. Joseph Donnelly,[13] Elisabeth A. Marley, Jeremy M. Milikow

As communication networks continue to increase in speed and bandwidth, the semiconductor industry must continue to strive to provide network designers with devices that will meet their needs. One of the more critical requirements is the need for optical devices that operate with little or no drive current so that they may operate, or cause another optical source to operate, at extremely high pulse rates.

Devices operating at wavelengths of 1.55 μm and 1.3 μm are the standard for optical communication networks because the low loss and zero dispersion propagation wavelengths for commonly used optical fiber are 1.55 μm and 1.3 μm, respectively. These wavelength requirements can be met using the III-V materials system, specifically (In,Ga)(As,P). The growth method used for this project is gas source molecular beam epitaxy. GSMBE combines the flexibility and the use of gaseous group V hydrides (AsH$_3$, PH$_3$) with the conventional molecular beam epitaxy control of the solid group III elements (In,Ga,Al). This combination lends itself to the growth of multi-layered structures, such as multiple quantum well (MQW) lasers and saturable Bragg reflectors (SBRs).

MQW lasers have become the preferred laser for communication networks due to the fact that they require a fewer number of injected carriers to operate than do separate confinement heterostruc-

ture (SCH) lasers.[14] For this reason, the threshold current of MQW lasers is lower than that of other lasers. By manipulating the doping levels in the laser as well as accurately controlling the heterojunctions, the threshold current can be decreased even further. In conjunction with Dr. Joseph Donnelly of MIT Lincoln Laboratory, the current design is a broad area laser that contains three quantum wells and a lightly doped upper InP cladding layer, e.g., approximately 5×10^{17} Be atoms/cm^2, in order to minimize the free carrier loss. The net gain versus current density and the device structure are shown in figure 8. This structure has yielded threshold current densities of 190 A/cm^2 for 3000 μm devices and a transparency current density of 165 A/cm^2. Current work on this topic includes fabricating and testing ridge waveguide lasers and tapers as well as designing future MQW laser structures.

Saturable Bragg reflectors (SBRs) are also of use in optical networks. SBRs are passive devices that are essentially distributed Bragg reflectors (DBRs). The SBR is designed as a conventional DBR, with a reflectivity bandwidth dependent upon the refractive indices and the thicknesses of the layers. The only difference is the incorporation of a single quantum well in one of the quarter-wave layers. The reflected intensity of this device, at the quantum well emission wavelength, can be varied based on the position of the quantum well within the DBR structure, e.g., the reflected intensity is highest if the quantum well is placed in the first quarter-wave layer, and decreases as the quantum well is placed further into the device. This quantum well should have an emission wavelength within the DBR reflectivity bandwidth in order to maximize the nonlinear reflectivity of the SBR due to the nonlinear effects caused by the quantum well. By placing the SBR in a low-gain solid-state laser cavity, its nonlinear reflectivity will mode-lock the laser, with the result being self-starting, stable, ultrashort optical pulses.[15]

SBRs have been demonstrated in the 0.85 μm wavelength range by Tsuda, et al.,[15] but this wavelength is not usable in standard optical networks, thus, the need for SBRs that operate at 1.3 μm and 1.55 μm. In order to accomplish this, a material system such as (In,Ga)(As,P) lattice-matched to InP must be used. The disadvantage of this material

[13] MIT Lincoln Laboratory, Lexington, Massachusetts.

[14] P.S. Zory, Jr., ed., *Quantum Well Lasers*, (New York: Academic Press, 1993).

[15] S. Tsuda, W.H. Knox, E.A. de Souza, W.Y. Jan, and J.E. Cunningham, "Low-loss Intracavity AlAs/AlGaAs Saturable Bragg Reflector for Femtosecond Mode Locking in Solid-state Lasers," *Opt. Lett.* 20(12): 1406-1408 (1995).
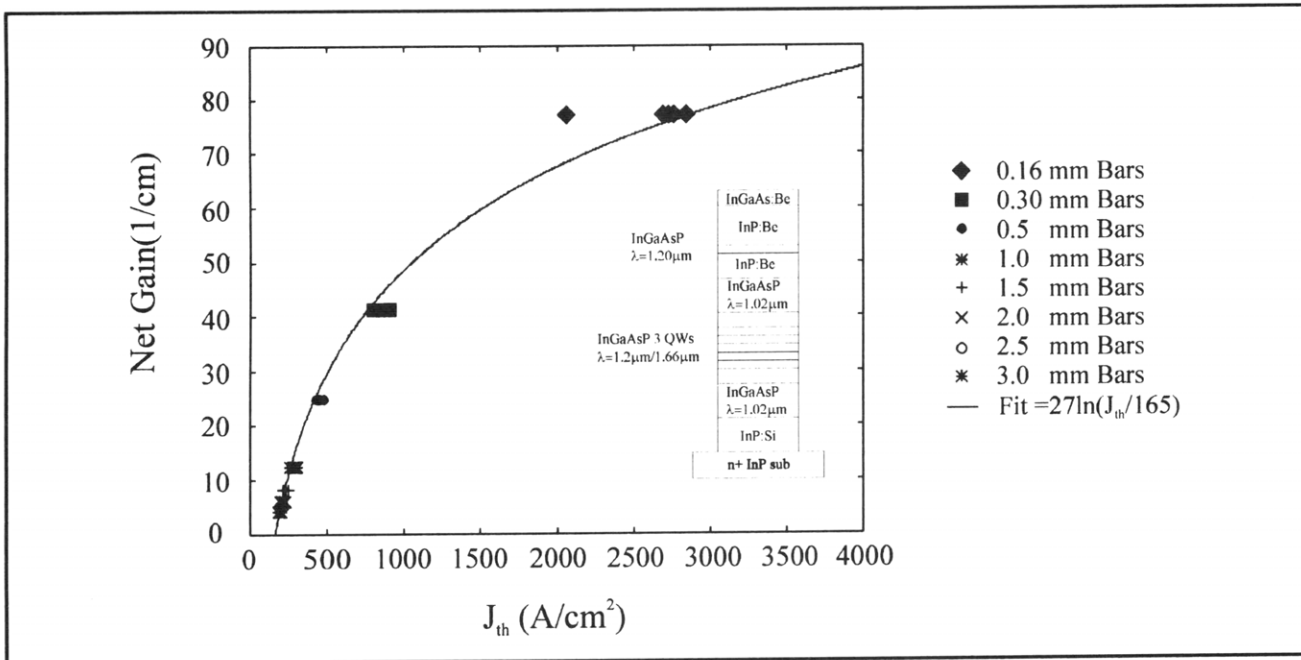
Figure 8. Net gain versus current density for 3 quantum well broad area lasers of various cavity lengths. The inset depicts the laser structure.

system is the small refractive index difference between (In,Ga)(As,P) and InP. To compensate for this, the SBR must contain on the order of 30 pairs of layers so as to achieve a reasonable reflectance. Due to the thickness requirements of each layer, this structure requires 15 or more hours for the GSMBE growth alone. When dealing with GaAs-based devices, it is possible to increase the difference in refractive indices by oxidizing AlAs. This increase in the difference between the high and low refractive indices in the DBR stack causes an increase of the stack reflectivity with fewer layers. For the InP system, the Al-containing compounds that are lattice-matched to InP are InAlAs and InAlAsP, which, when unoxidized, have a refractive index comparable to InGaAsP. Current work on this topic involves the oxidation of InAlAs(P) in a DBR-type structure.

3.7 Integrated Optical Filters and Circuits in InP

Sponsors

MIT Lincoln Laboratory
National Center for Integrated Photonic Technology
    Subcontract 542-383

Project Staff

Professor Hermann A. Haus, Professor Leslie A. Kolodziejski, Professor Henry I. Smith, Dr. Gale S. Petrich, Jay N. Damask, Elisabeth A. Marley, Jeremy M. Milikow

As the designs for the integrated-resonant channel-dropping filter (CDF) have matured over the last year, increasing emphasis has been placed on the structural properties and integrity of the waveguides and gratings. In particular, an "ideal" CDF, made in the (In,Ga)(As,P)/InP material system, uses a quaternary alloy with a dilute concentration of Ga and As ($In_{0.93}Ga_{0.07}As_{0.15}P_{0.85}$), a rib height of about 1.5 μm, and a grating depth of about 0.7 μm which, at a 244 nm period, translates to a grating aspect ratio on the order of 6:1. These waveguide dimensions and core alloy concentration were derived from trading off the core-to-clad index contrast with feature size. Such a trade-off maintains the grating strength and the modal confinement required by the channel-dropping filters while decreasing the polarization dependence by over a factor of six from the previous designs and increasing the circularity of the mode which, in turn, increases the fiber-to-chip coupling. Moreover, the waveguides with the aforementioned parameters are channel guides, which means that the tolerance on the rib etch depth is no longer an issue because the rib can be etched to any depth into the lower cladding without changing the optical properties.

The primary drawback to the current design is the high aspect ratio gratings. Such gratings will pose challenges to the etching, the thermal cleaning process, and the overgrowth steps that are required for fabrication. Reactive-ion etching is a popular

method to anisotropically etch high aspect ratio features, but optimizations to the process will have to be undertaken to insure that the grating tooth profile has straight side walls. After feature definition, the wafer must be returned to the GSMBE reactor for the growth of the upper InP cladding layer. Conventionally, in order to remove the native oxide and other contaminants from the surface, the wafer is thermally cleaned in the reactor. However, such treatment will likely cause some degree of reflow of the gratings which will dramatically degrade the spectral response of the CDF filter. In order to circumvent the thermal desorption of the oxide, a new atomic hydrogen source has been installed into the growth reactor. The atomic hydrogen species can remove the oxygen and carbon containing contaminants on the wafer surface at temperatures around 300°C. This cleaning treatment will likely pave the way in order to retain the structural integrity of the grating features.

Nucleation and full overgrowth of the grating features, with their 6:1 aspect ratios, has not been investigated. In order to understand the effects that influence the growth process, electron-beam lithography will be used to directly write features of various periods, duty cycles, and crystalline orientations. After each overgrowth on a patterned wafer, a focused-ion-beam tool will be used to create cross-sections of the grating with overgrowth for closer inspection.

In order to control the core alloy concentration in real time during the course of the film growth, an *in situ* ellipsometer is being installed on the GSMBE system. The feedback from the ellipsometer will be used to insure that the film composition is uniform and that the target thicknesses of the core and etch-stop layers are met to within ± 0.5 percent.

The combination of atomic hydrogen surface cleaning, *in situ* composition and thickness control, and focused-ion-beam work, in addition to waveguide designs, layout and nanolithographies, will, at the very least, offer a wide range of possible solutions to meet the specifications of the "ideal" channel-dropping filter design.

3.7.1 Publications

Damask, J.N. "Practical Design of Side-Coupled Quarter-Wave Shifted Distributed-Bragg Resonant Filters." Submitted to *J. Lightwave Tech.*

Damask, J.N. "Design of Synchronous Integrated-Optical Side-Coupled Resonators." Submitted to *J. Lightwave Tech.*

3.8 Photonic Bandgap Structures

Sponsor

Project Staff

Professor John D. Joannopoulos, Professor Leslie A. Kolodziejski, Professor L. Rafael Reif, Dr. Gale S. Petrich, Dr. Pierre Villeneuve, Kuo-Yi Lim, Shanhui Fan, Jerry C. Chen, Xiao-feng Tang

A photonic crystal is a periodic dielectric structure that presents a range of frequencies within which photons fail to propagate. This forbidden band of frequencies translates into a photonic bandgap (PBG), analogous to an electronic bandgap in a semiconductor crystal. A defect state can also be introduced in the photonic bandgap when the dielectric periodicity of a photonic crystal is broken by the selective removal or addition of dielectric material. This defect results in the spatial localization of the defect mode to within a volume of approximately one cubic wavelength, yielding a high-Q electromagnetic microcavity. The realization of such a microcavity holds promises of vastly reducing spontaneous emission and zero point fluctuations within an energy band.

The main problem with the microfabrication of a three-dimensional photonic crystal originates from the rather sophisticated geometry and intricate arrangement of holes and rods needed to open a bandgap. These complex structures do not easily lend themselves to fabrication at submicron lengthscales. For example, the three dimensional PBG structure that is under investigation, is made of three materials (Si, SiO_2, and air) and consists essentially of a layered structure in which a series of cylindrical air holes are etched at normal incidence through the top surface of the structure. Furthermore, most applications for photonic bandgap structures require bandgaps larger than 10 percent which in turn require the use of materials with large index contrasts such as in the case of Si and SiO_2. In the structure under fabrication, the photonic bandgap is as large as 14 percent of the midgap frequency using Si, SiO_2, and air; and 23 percent using Si and air (after the SiO_2 is etched away). Until now, three-dimensional PBG crystals have been constructed for operation in the millimeter

wave region,[16] and the fabrication of a two-dimensional photonic bandgap nanostructure has been reported.[17]

Several difficulties arose during the fabrication of the three-dimensional photonic bandgap structures. The first difficulty was creating Si trenches with the correct geometry. This problem was alleviated by using a low temperature oxide (LTO) as a hard mask as opposed to a photoresist mask and by the use of a special Cl_2 plasma etch. The second difficulty was the creation of voids in the SiO_2 that was subsequently deposited into the Si trenches using a LTO or SiO_2 that was deposited by plasma-enhanced chemical vapor deposition. Using 1 μm of boron phosphide silicate glass along with 1 μm of LTO, the Si trenches were completely filled with SiO_2 after the chemical/mechanical polishing step. Figure 9 shows the completed first layer. The third difficulty that arose was in the creation of a reproducible 1 μm shift between the second layer Si trenches and the first layer Si trenches. Future work includes the completion of the ten layers that are needed in the three-dimensional photonic crystal and the verification of the photonic bandgap.

The photonic bandgap air-bridge microcavity is essentially a one-dimensional photonic crystal made of III-V compound semiconductor material (refractive index, n~2.9-3.3) surrounded by air (n=1.0). The one-dimensional crystal comprises of a semiconductor bridge that is punctuated with holes that are periodically spaced along the length of the bridge. A defect is introduced into the crystal by removing one of the holes. In *Progress Report No. 137*, we reported the successful fabrication of these structures using both silicon-based and III-V semiconductor material. Since that report, we have proceeded to design and fabricate devices coupled with single-mode waveguides for measurement purposes. These photonic bandgap air-bridge devices have been designed to exhibit a photonic bandgap centered at a wavelength of 4.5 μm.

A typical device consists of a photonic bandgap air-bridge with waveguides feeding into and leading out of the air-bridge. The air-bridge material is GaAs and the structure is typically 14 μm long, 1.8 μm wide and 0.4 μm thick. The holes are 1.0 μm in diameter and are separated by 0.8 μm. (The period of the holes is 1.8 μm.) The defect is 2.6
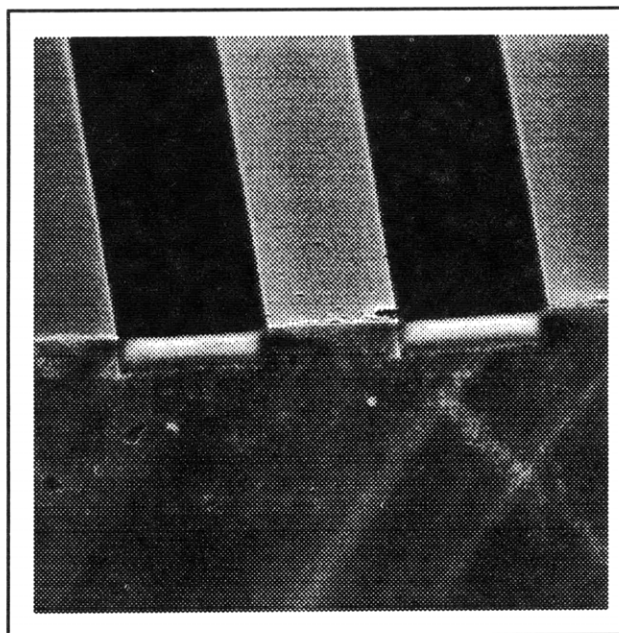
Figure 9. Scanning electron micrograph of the completed first layer of a three-dimensional photonic bandgap structure. The Si trenches are 1.8 μm wide and 1 μm deep.

μm wide (measured center-to-center of the two holes bordering the defect). The waveguide material is also GaAs, but has an upper cladding layer of $Al_{0.3}Ga_{0.7}As$ and a lower cladding layer of $Al_{0.7}Ga_{0.3}As$. The material configuration is designed to enhance the coupling of both the input beam from free space into the input waveguide, and from the input waveguide into the photonic bandgap air-bridge. Typically, the upper cladding is 0.4 μm thick and the lower cladding is 0.4 μm thick, and the tri-layer waveguide structure sits on a 4 μm $Al_{0.9}Ga_{0.1}As$ layer on top of the GaAs substrate.

The initial compound semiconductor material for the photonic bandgap air-bridge structure is grown by gas-source molecular beam epitaxy in the Chemical Beam Epitaxy Laboratory. A series of high-resolution photolithography, reactive ion etching and wet chemical etching steps are then performed to fabricate the bridge and waveguide structures. These processing steps utilize the facilities in both the Microsystems Technology Laboratory and the Center for Material Science and Engineering Microelectronics Fabrication Laboratory. We have successfully fabricated these devices and a scanning

16 E. Özbay, E. Michel, G. Tuttle, R Biswas, K.M. Ho, J. Bostak, and D.B. Bloom, "Double-etch Geometry for Millimeter-wave Photonic Band-gap Crystals," *Appl. Phys. Lett.* 65(13): 1617-1619 (1994).

17 P.L. Gourley, J.R. Wendt, G.A. Vawter, T.M. Brennan, and B.E. Hammons, "Optical Properties of Two-dimensional Photonic Lattices Fabricated as Honeycomb Nanostructures in Compound Semiconductors," *Appl. Phys. Lett.* 64(6): 687-689 (1994).

electron micrograph of such a device is shown in figure 10.
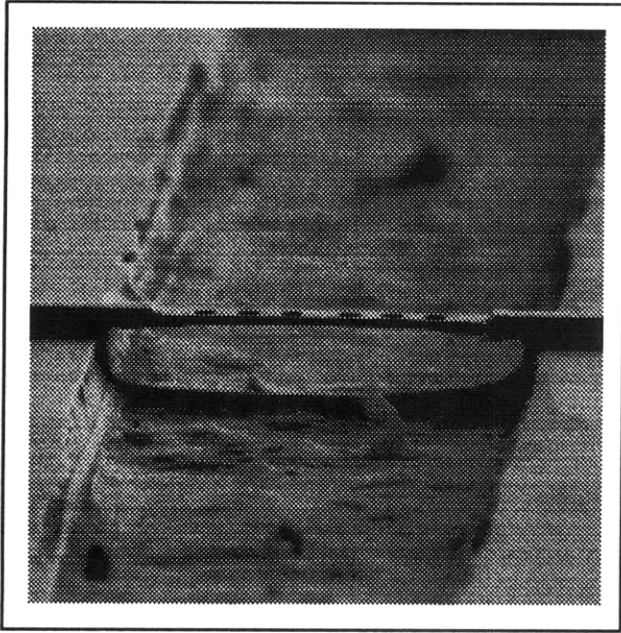
Figure 10. Scanning electron micrograph of a photonic bandgap air-bridge device coupled with input and output waveguides. The air-bridge is 1.8 μm wide, 0.4 μm thick and approximately 14 μm long. The holes are 1.0 μm in diameter and are separated by 0.8 μm. The defect region, in the middle of the air-bridge, is 2.6 μm wide (center to center). The 0.4 μm thick upper cladding layer of the waveguide (absent from the bridge) is clearly visible.

An experimental optical setup to measure and characterize the photonic bandgap air-bridge structure is under construction and measurements will be performed in the near future in conjunction with Professor Erich Ippen's group.

3.8.1 Publications

Villeneuve, P.R., S. Fan, J.D. Joannopoulos, K.Y. Lim, G.S. Petrich, L.A. Kolodziejski, and R. Reif. "Air-Bridge Microcavities." *Appl. Phys. Lett.* 67(2) 167-169 (1995).